



Universiteit
Leiden
The Netherlands

Development and testing of the gravitational wave antenna MiniGRAIL in its full-featured configuration

Usenko, O.

Citation

Usenko, O. (2012, May 23). *Development and testing of the gravitational wave antenna MiniGRAIL in its full-featured configuration*. *Casimir PhD Series*. Retrieved from <https://hdl.handle.net/1887/18979>

Version: Not Applicable (or Unknown)

License: [Leiden University Non-exclusive license](#)

Downloaded from: <https://hdl.handle.net/1887/18979>

Note: To cite this publication please use the final published version (if applicable).

Cover Page



Universiteit Leiden



The handle <http://hdl.handle.net/1887/18979> holds various files of this Leiden University dissertation.

Author: Usenko, Oleksandr

Title: Development and testing of the gravitational wave antenna MiniGRAIL in its full-featured configuration

Date: 2012-05-23

Chapter 3

Preparing for the first scientific run

Introduction

In this chapter we summarize all the improvements we have made to the MiniGRAIL setup in the process of the preparation for a full 6-transducer scientific run. Every intermediate run we had, contributed to our experience and understanding of problems we might face during the course of the experiment. The major improvements are listed below, and explained in details in the rest of the chapter.

- We believed that a structural imperfection of the first MiniGRAIL sphere was limiting the mechanical quality factor of the modes, so it was replaced with a new one. The new sphere is also slightly bigger in diameter - 68 cm instead of 65 cm , the maximum size that fits in the Dewar of MiniGRAIL setup. The old sphere was annealed at $400\text{ }^{\circ}\text{C}$ on air, while the new one was annealed at a temperature of $800\text{ }^{\circ}\text{C}$ in vacuum in order to decrease the concentration of internal defects that could lead to long thermal relaxation times at mK temperatures.
- New improved capacitive transducers were designed all coupled to a superconducting transformers and a double stage SQUID amplifiers.
- A complete data acquisition system was developed and installed. We have also developed some basic data processing software(see chapter 2). The stability of the detector's acquisition system was also studied.
- Based on the results of the previous experiments, we improved the magnetic shielding of the setup and installed radio frequency filters on the electric lines, going to the sphere from room temperature.

3.1 New transducers design

In order to increase the sensitivity, we have designed new transducers with a larger electrode area and smaller resonant mass. They were also designed in a way that greatly simplifies the polishing of a capacitor surface thus increasing the maximum electric field the transducer can hold.

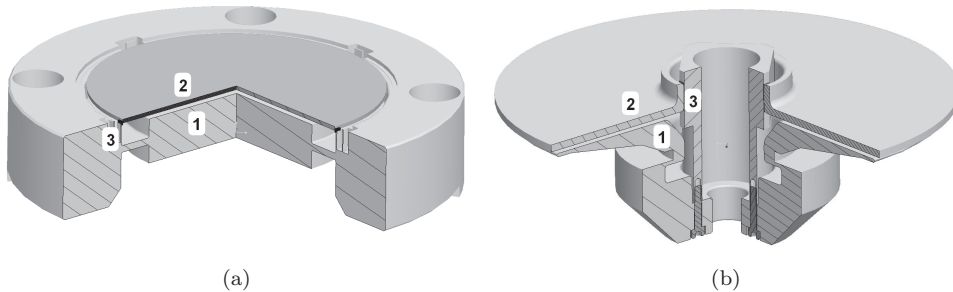
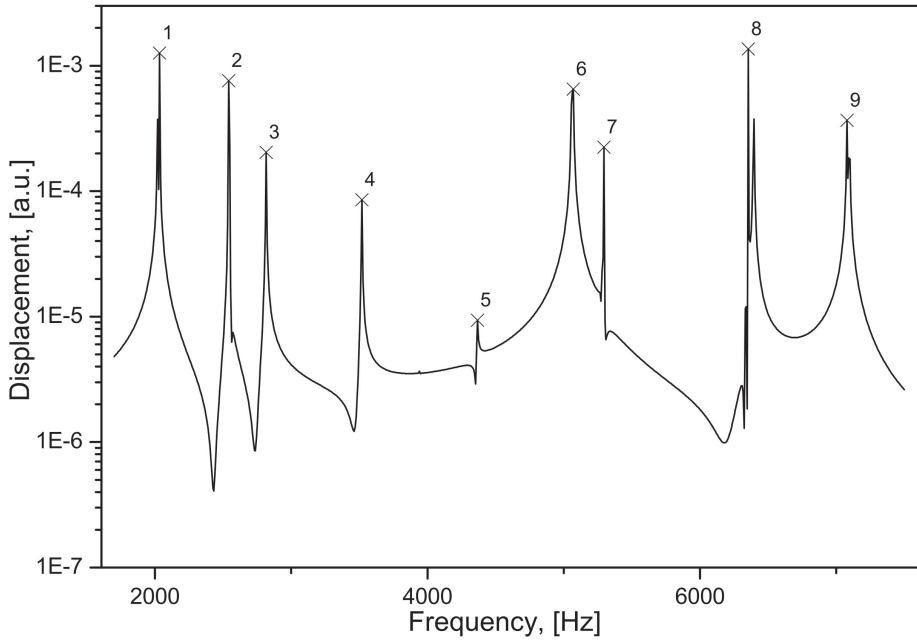


Figure 3.1: Transducers design - old(a) and new(b). The electrode(2) is glued with insulating epoxy to the support(3) forming a planar capacitor with a resonating mass(1).

In the old “closed membrane” [25] transducer design on figure 3.1(a) the resonating mass (1) is machined together with the electrode support (3) and is lower than the surrounding transducer body thus making the polishing of the resonator surface a complicated task. Also once the transducer is assembled it is not possible to open it again for cleaning without removing the epoxy and regluing the electrode again afterwards.

In the new design on figure 3.1(b) the electrode support is attached to the transducer body by means of 4 M3 screws and can be easily removed, so the capacitor surfaces can be polished very well. After the mass and the electrode are polished, the support is installed in place and the electrode is glued to it with Stycast 2850FT epoxy. A $15\ \mu\text{m}$ Kapton foil is used as a spacer to create the gap between the electrode and the resonating mass. It is also possible to disassemble the transducer to clean the electrodes and assemble it again without significant change in transducer capacitance or planarity. As can be seen from table 3.1 due to the smaller gap and much larger surface area the capacitance of the new transducers is almost a factor of 5 higher than of the old ones.

Since making a real transducer is a precise and time consuming work, before the actual machining we always evaluate the design by performing a Finite Element Analysis (FEA) study. On figure 3.2 the results of the resonator modal analysis are shown. The mechanical properties of the model are set to match CuAl6\% and the bottom surface is set fixed. It is easy to see that the only mode that couples well to the radial motion of the sphere is the $2816\ \text{Hz}$ “umbrella” mode of the electrode.



01 - 2033Hz



02 - 2541Hz



03 - 2816Hz



04 - 3519Hz



05 - 4368Hz



06 - 5071Hz



07 - 5296Hz



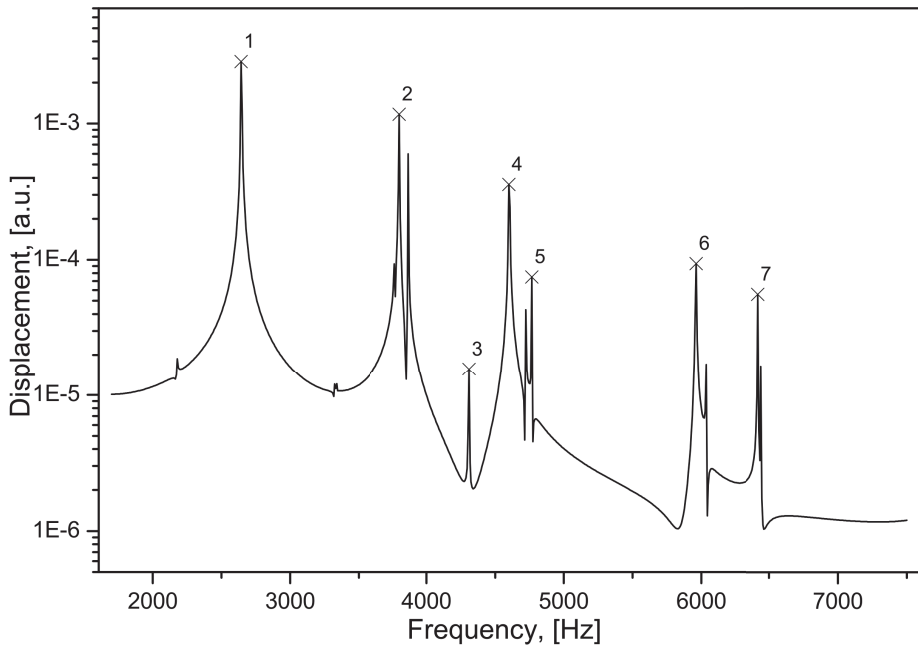
08 - 6354Hz



09 - 7079Hz



Figure 3.2: Resonator FEA simulation



01-2642Hz



02-3802Hz



03-4310Hz



04-4600Hz



05-4766Hz



06-5963Hz



07-6419Hz



Figure 3.3: Electrode FEA simulation

Parameter	old transducers	new transducer
mass, [kg]	0.2 – 0.7	~ 0.2
area, [cm ²]	~ 25	100
gap, [μ m]	25 – 50	15
C, [nF]	≤ 1	4 – 5

Table 3.1: A comparison of the properties of the old transducers, used in previous runs and the improved design (new transducer). The increased area and the smaller gap of the new transducer results in a capacitance of about a factor of 5 higher than that of the old transducers type.

This is also the only mode that significantly changes the average distance between the resonator and the electrode, thus modulating the transducer capacitance.

On a real transducer it is possible to tune the frequency of the “umbrella” mode by slightly varying the shape of the resonator.

We have also performed a study of the electrode assembly (see figure 3.3). We have found one mode that might lie in the bandwidth of MiniGRAIL - 2858 Hz mode, but because it is a bending mode it should weakly couple to the radial motion of the sphere and since the electrode is glued to the support by means of low Q epoxy glue, the mechanical quality factor of the assembly should be low.

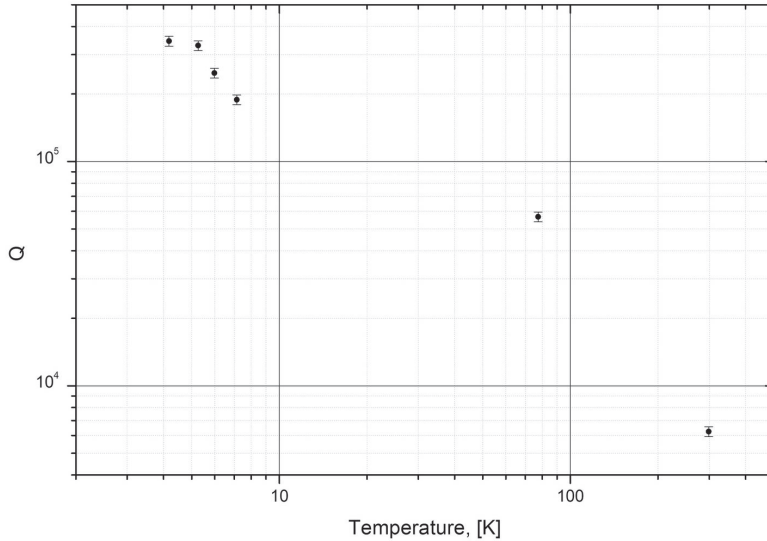


Figure 3.4: Mechanical quality factor of the “umbrella” mode of the transducer as a function of the temperature. The transducer was assembled with a gap of $\sim 25 \mu\text{m}$ and was charged to 180 V.

We have measured the mechanical quality factor of the assembled transducer down to the temperature of 4.2 K . During the test the transducer was suspended in high vacuum inside a 4 K cryostat. The transducer was assembled with a gap of $\sim 25\text{ }\mu\text{m}$ and was charged to 180 V . We used a small piezoelectric actuator glued to the support of the transducer to excite the resonator and an amplifier connected to the transducer through the decoupling capacitor for read-out. The Q factor was calculated from the ring-down measurement.

The mechanical quality factor of the 2953.4 Hz “umbrella” mode of the resonator as a function of temperature is shown on figure 3.4. At 4.2 K the quality factor we have measured is $\sim 3 \times 10^5$, which is at least on a par with the previous transducers designs. We have also noticed that the Q factor decreases with the increase of the transducer bias voltage, yielding [51] the electric quality factor $Q_{el} \sim 15 - 20$. This value indicates high electric losses in the transducer. The origin of such losses is unclear, however for every transducer design we had, Q_{el} was always in the same range.

3.1.1 Transducers bias voltage stability

The stability of the transducers charge was one of the problems we encountered during the previous runs. Because of the high mechanical quality factor of the modes, it might take many hours to accurately acquire the data with enough resolution and signal to noise ratio to make the calibration. The electric field in a transducer gap introduces an attractive force between the electrode which reduces the mechanical spring constant of the resonator. A change of the resonance frequency of the mode due to changed spring constant can be expressed as $f_r^2 = f_0^2 + \alpha V_b^2$ [25], where V_b is the bias voltage of the transducer, and α is the coupling factor which expresses how well the transducer is coupled to the particular resonance mode. Thus if V_b drifts with time, it is not possible to acquire the modes accurately.

A capacitive transducer can lose the charge due to current leakage between the electrode and the resonating plate or through the voltage bias line connected to the transducer. The high resistance of Stycast epoxy, used to assemble the transducer, and high vacuum in the IVC prevent the current leakage between the plates. To prevent the discharging through the bias line we use magnetic reed switches (see fig. 3.5(a)). The switches are normally open, so they mechanically disconnect a transducer from the bias line¹.

The figure 3.5(b) shows the evolution of the resonant frequency of the modes during one week period of 8 September - 16 September 2005. The bias voltage was 192 V . As an example we have also plotted the data from 27 September which is acquired with a bias voltage of 204 V and shows a clear frequency shift. So, as we can see, no noticeable transducer discharge observed for one week of monitoring.

¹When using reed switches at low temperatures one should pay attention that some switches might have an exchange gas inside which condenses on the electrode and freezes the switch open.

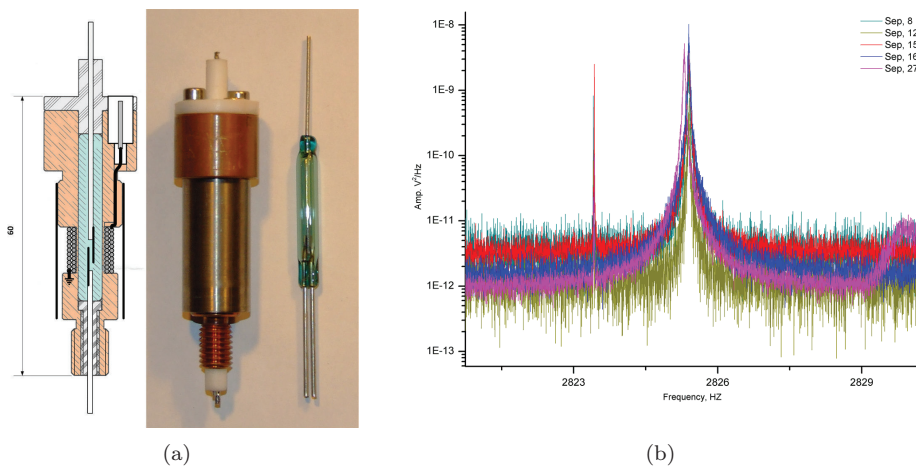


Figure 3.5: Reed switch used to physically decouple the charging line from the transducer (a) and modes frequencies evolution with time (b). Transducer bias voltage was 192V for September 8 - September 16 and 204V for September 27 2005

3.2 New superconducting transformers

In order to efficiently couple the low impedance SQUID input coil to a high impedance capacitance transducer an impedance matching transformer has to be used. We have redesigned the superconducting matching transformer housing in order to fit six of them on the last mass of the vibration isolation system.

The design is similar to the one of the old transformer box reported in [25]. The housing(1) is made of lead-plated copper and has three separate compartments for the superconducting transformer(2), decoupling low loss Teflon capacitor(3) and double compartment for the SQUID modules(4). The transformer is placed inside an extra lead-plated copper box(5), wrapped in cryoperm foil, and placed inside the main box. A small transformer(6) is placed in-between the secondary coil of the matching transformer and the input coil of the SQUID. It is used to inject a calibration signal to the SQUID input in order to calibrate the SQUID amplifier sensitivity. The decoupling capacitor is needed to separate the SQUID input from a high DC bias voltage of the transducer. The design properties of the transformer box are summarized in table 3.2

3.2.1 Connecting input terminals of the SQUID

A common technique to connect the input terminals of the thin-film SQUID module to the PC-board is by means of the ultrasonic bonding. For bias and Fb lines it is possible to use the standard Al bonding wire. However for the input terminal of the SQUID a superconducting wire has to be used. We use a $50\mu\text{m}$ Nb wire annealed and

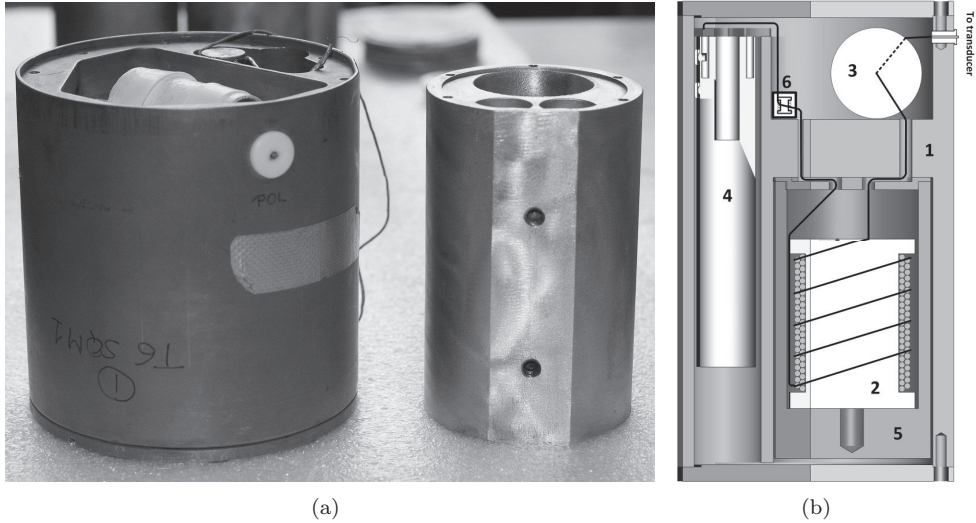


Figure 3.6: New superconducting transformers, (a)-compared to the old design, (b)-schematics: 1-Lead-plated Cu housing, 2-Superconducting matching transformer, 3-decoupling capacitor, 4-SQUID module, 5-Transformer housing, 6-Calibration transformer

Primary Inductance, $[H]$	0.2
Secondary Inductance, $[\mu H]$	2
Coupling	0.85
Electric mode Q	$\geq 5 \times 10^4$
Calibration coil mutual inductance, $[nH]$	100
Decoupling Capacitor, $[nF]$	150/136

Table 3.2: Transformer box design parameters.

etched with 1:1 HF and HNO₃ mixture to the thickness of 15 – 20 μm . The annealing is done in vacuum. The wire is heated to a temperature of $\simeq 2200^\circ C$ by sending a current through it for a time of about 5 min . As a result we get very plastic bonding wire with a critical current of the bonds about an order of magnitude higher than the dynamic range of the SQUID and a thermal noise much lower than the internal noise of the SQUID.[52]

3.3 Magnetic Shielding

In order to reduce the magnetic noise picked up by the SQUIDS, 50mK and Still flanges together with the corresponding radiation shields were lead-tin plated. To reduce the trapped magnetic field, the shields were also covered by a few layers of

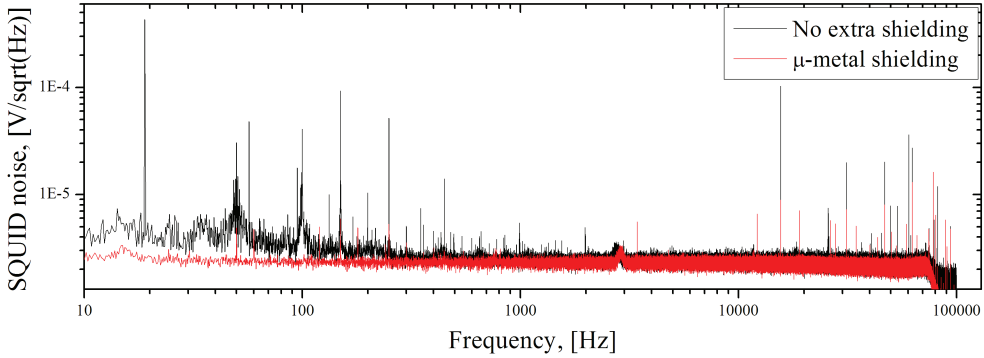


Figure 3.7: Effect of the magnetic shielding on the SQUID noise

high magnetic permeability μ -metal foil. The effect of the magnetic shielding on the SQUID noise measured on a dipstick is shown on figure 3.7.

3.4 RF filters

We have developed compact copper powder RF filters that will be installed on the calibration lines at low temperatures, so the RF noise picked up by the cables will not interfere with the SQUID operation. At frequencies below 1 MHz , we have measured

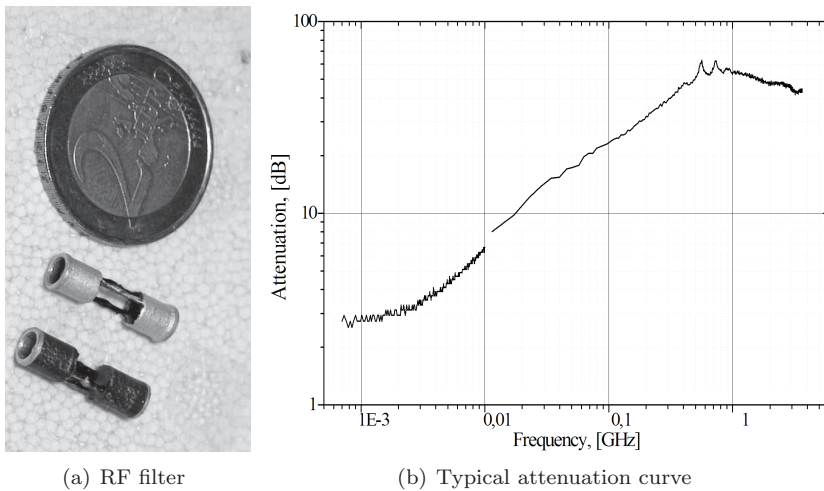


Figure 3.8: A design and attenuation curve of copper powder RF filters we have developed

the attenuation of less than 3 dB , which is acceptable in our case. Above the frequency of 500 MHz the attenuation increases to $45 - 55\text{ dB}$ (see figure 3.8). We have found that it is possible to increase the attenuation up to $90 - 100\text{ dB}$ by using a smaller gauge wire with thinner insulation, but the reliability and the yield drops to unacceptable values.

3.5 SQUID developments

3.5.1 Run 8 acquisition stability

Run8 was the first one where the sphere was operated for a relatively long time at millikelvin temperatures. It lasted for three months - from beginning of August 2005 till mid November 2005. The overview of the data acquisition activity is presented on figure 3.9

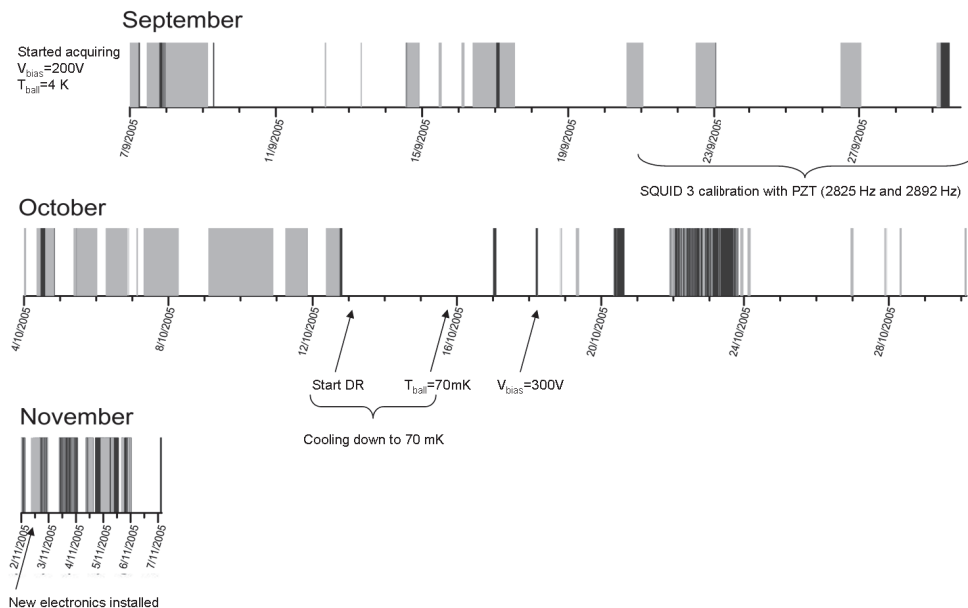


Figure 3.9: Run8 data acquisition overview. Gray regions show when the acquisition was running with light gray color meaning that the sphere modes were visible above the SQUID noise

The overview is made offline by analyzing the acquired data for the visibility of the normal modes of the sphere. The light gray color indicates that the modes are visible in the noise spectra and their SNR is above a threshold. The dark gray color indicates that the system was running and SQUIDs were locked, but the modes were

not visible. White color means that the acquisition was not running.

	September	October	November
Duty cycle, [%]	25	33	56
Good data, [%]	84	64	22

Table 3.3: MiniGRAIL duty cycle during run8

As we can see from the table 3.3 the duty cycle of MiniGRAIL during Run8 was not very big, especially in September. This is due to some non data acquisition works (like transducers calibration), which were conducted during the run. However, when the acquisition was running, the amount of good data was high enough during the first two months of operation but dropped dramatically in November, when the antenna was cooled to a temperature below 70 mK. We believe that the reason might be in the SQUID we used for the second stage. The steep flux-voltage transfer of the DROs makes them a good choice for an amplifier SQUID [25, 48]. Because of the large gain direct readout electronics can be used, which simplifies the electronics design a lot. However, our experience has shown that the high flux-voltage gain of the DROS can also cause the stability problems, especially at low temperatures when the gain increases even further. This is believed to be a reason of a very low stability of MiniGRAIL acquisition below 4 K, described above.

Because of problems operating the DROs at mK temperatures we decided to switch back to a conventional DC SQUID as an amplifier. The SQUIDs were developed by Low Temperature division of the Department of Applied Physics at the University of Twente and are fabricated at a foundry of IPHT Jena [53]. The 4.2 K measurements were performed in Leiden and Twente universities. Millikelvin measurements were done in a dilution refrigerator at Leiden Cryogenics [54]

The SQUIDs are designed using the maximal line width resolution available by the process - $3 \mu m$. The size of the Josephson junctions is $3.2 \times 3.5 \mu m^2$ and the critical current density J_0 was $110 A/cm^2$ and $120 A/cm^2$. The critical current density tolerance across the single chip is 5%. The Josephson junctions are externally shunted by shunt resistors made of resistive 115 nm PdAu film. The SQUID chip dimensions are $2.5 \times 2.5 mm^2$. Two different SQUID layouts were made - flux transformer and parallel washer design SQUIDs. The design considerations, model, and the experimental results are explained in detail in [55]. Here we will only give a summary of the key parameters of the SQUIDs.

3.5.2 Flux transformer DC SQUID

The aim of the flux transformer design is to couple a low inductance SQUID loop ($L_{SQ} \sim 10^2 pH$) to a high inductance input coil ($L_{inp} \approx 1.6 \mu H$), used in MiniGRAIL read-out, by means of an intermediate transformer. To overcome resonance effects, a damping resistor, R_d is added in parallel to the SQUID loop. It has the same resistance as the

shunt resistors of the Josephson junctions ($5.7\ \Omega$). The schematics and the layout of the flux transformer SQUID are shown on the figure 3.10. The design parameters are summarized in the table 3.4

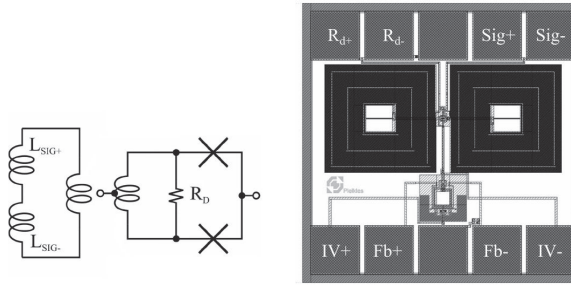


Figure 3.10: Twente Flux transformer SQUID schematics [a] and layout [b]

	$2I_0, \mu A$	R_{sh}, Ω	L_{sq}, pH	β_L	β_C	$L_{sig}, \mu H$	M_{sig}, nH
Design	22.6	5.7	170	1.8(1.1*)	0.7	1.6	10.4
Measured	24	5.0		1.9(1.2*)	0.6		8.7

* - at RF frequency

Table 3.4: FT SQUID design parameters

Using the theory for non hysteretic, uncoupled DC SQUIDS [26] we can estimate the best reachable sensitivity. For a temperature of $4.2\ K$ the calculated flux noise spectrum density is $S_\Phi = 0.68\ \mu\Phi_0/\sqrt{Hz}$ corresponding to an energy resolution of $73\ \hbar$.

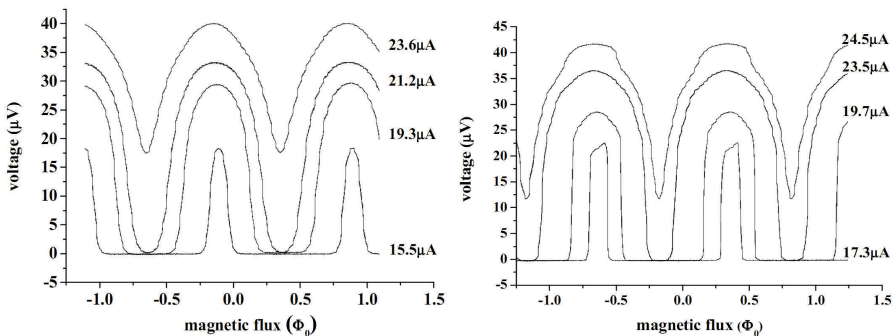


Figure 3.11: A flux-voltage characteristics of a FluxTransformer SQUID at $4.2\ K$ (a) and $300\ mK$ (b)

The measured flux-voltage characteristics of the SQUID at two different temperatures are shown on figure 3.11. At 4.2 K, we observed a maximum flux-voltage transfer of $110 \mu\text{V}/\Phi_0$ - 2.5 times the value predicted by the theory [26]. At 0.3 K it has increased to $\approx 800 \mu\text{V}/\Phi_0$. The measured mutual inductance of the input coil is 8.7 nH instead of the design value of 10.9 nH. A minimum flux noise of $1.4 \mu\Phi_0/\sqrt{\text{Hz}}$ was measured at 4.2 K in a two-stage setup with a DROS as second stage. Because of the steep transfer function at low temperatures we did not succeed in getting a two-stage setup working. In a single stage a flux noise of $2.8 \mu\Phi_0/\sqrt{\text{Hz}}$ was achieved at temperatures below 1 K. By subtracting the flux noise related to the room temperature amplifier from the measured value, the rough estimation of the real flux noise below 1 K is $1.5 - 2 \mu\Phi_0/\sqrt{\text{Hz}}$.

3.5.3 Parallel washer DC SQUID

Because of its symmetric layout and the reduced coupling between the feedback- and the signal-coils, this design was made similar to the one of a commercial Quantum Design SQUID [56].

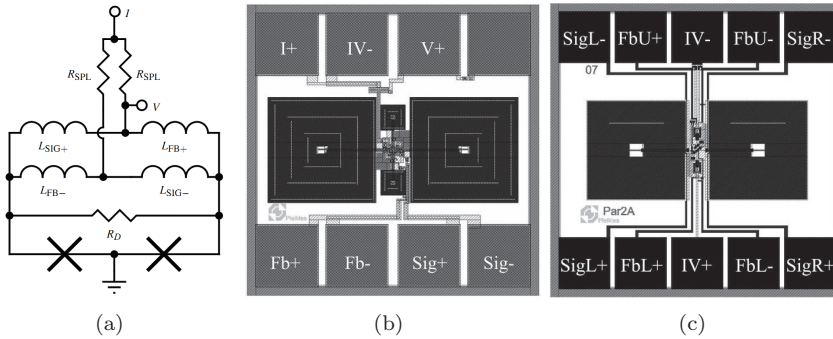


Figure 3.12: Parallel washer design SQUID schematics (a) and layout of first (b) and second (c) design steps

The layout and the schematic are shown on figure 3.12. The main differences from the original design are added cooling fins and the splitting of the bias current is done on-chip via the two parallel resistors R_{SPL} . The design parameters are listed in table 3.5.

We have measured the SQUID sensitivity with a dilution refrigerator in two-stage configuration. The Flux Transformer SQUID described above was used as an amplifier. The measured flux noise as a function of temperature is presented on figure 3.14

As we can see from the graph, the noise scaled almost linearly with the temperature down bath temperature of 600 mK . At 4.2 K we measured a flux noise of $2.1 \mu\Phi_0/\sqrt{\text{Hz}}$. Below the temperature of 200 mK , the measured flux noise was

	$2I_0, \mu A$	R_{sh}, Ω	L_{sq}, pH	$L_{inp}, \mu H$	M_{sig}, nH	β_L	β_C
Design	22.6	5.6	270	1.5	12.4	2.9(1.6*)	0.65
Measured	11	4.9			11.2	2.8(1.6*)	0.5

* - at RF frequency

Table 3.5: Parallel washer SQUID design parameters

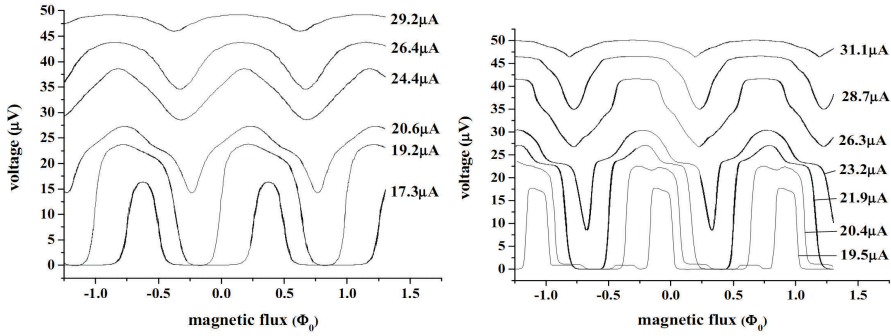


Figure 3.13: A flux-voltage characteristics of a parallel washer SQUID at 4.2 K (a) and 600 mK (b)

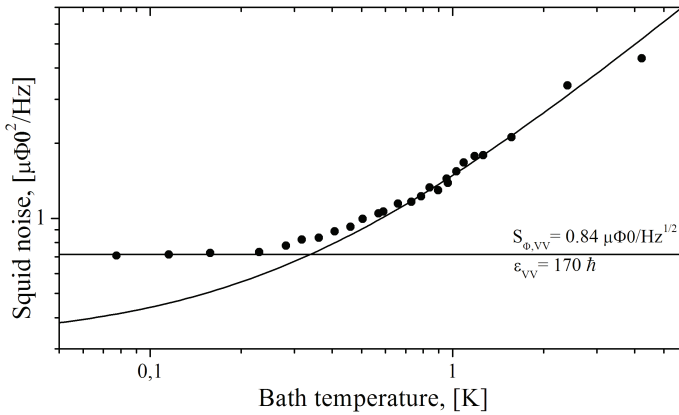


Figure 3.14: Flux noise of the parallel washer design SQUID as the function of temperature

$0.84 \mu\Phi_0/\sqrt{Hz}$ and did not improve further with temperature. This corresponds to an equivalent input noise current of $\sqrt{S_{\Phi, VV}}/M = 155 fA/\sqrt{Hz}$. Using the measured value of M and the design value of L_{inp} the coupled energy resolution $\epsilon_{vv} = 170 \hbar$.

The minimal effective temperature of about 400 mK was reached is due to the

influence of hot electron effect in the shunt resistors. The power dissipated in the resistors was estimated from the voltage and the bias current at the working point of the SQUID ($I_b \approx 30 \mu A$, $V \approx 40 \mu V$). Assuming that all the power dissipated only at the shunt resistors, $P = 0.6 nW$ per resistor, This value and the minimal reached effective temperature agrees with the model described in [55]

3.5.4 SQUIDs performance at mK temperatures

As we know, the noise of the typical DC SQUIDs we use in our experiments is dominated by the Johnson noise in the shunt resistors[26]. While it sounds promising, as the noise goes down with temperature, in practice there is a limit where dissipated power and a reduced electron-phonon interaction in a shunt resistor prevents it from further cooling. One of the thermal resistance mechanisms that one should often consider at low temperatures is boundary (Kapitza) resistance. It appears due to the acoustic phonon mismatch on the interface of two materials [57]. The relation between the dissipated power P and the temperature is

$$P = kA_k(T_{ph}^4 - T_{bath}^4), \quad (3.1)$$

where T_{ph} is the temperature of phonons in a shunt resistor, T_{bath} is the temperature of the thermal bath, A_k is the interface area, and k is a materials constant. A second thermal resistance mechanism is related to the electron-phonon interaction in the resistor itself. We can write down a similar relation for electron and phonon systems temperature:

$$P = \Omega\Sigma(T_e^p - T_{ph}^p), \quad (3.2)$$

where Ω is the resistor volume and Σ is constant which depends on the strength of electron-phonon coupling. The theoretically predicted value of the exponent $p = 4 - 6$ depending on the metal type and the phonon dimensionality. Experimentally in many cases $p = 5$. As we can see from equation 3.2 the obvious way to reduce the temperature difference for the same dissipated power is to increase the volume Ω . Extensions to the shunt resistors that increases the volume without changing the electrical resistance are called cooling fins.

The experiments to measure the effective temperature of shunt resistors as a function of the dissipated power and cooling fin size were performed in a dilution refrigerator in Leiden. The scheme of the experiment is shown on figure 3.15. The shunt resistor R_d is biased by a low-pass filtered ($C_{LP} = 1 \mu F$, $R_{LP} = 760 k\Omega$) current source I_b . The power, dissipated on a resistor is $P = I_b V$, where V is the voltage drop across the resistor, measured by a room temperature voltmeter, connected in a four-terminal scheme. The temperature of the resistor is evaluated by measurement of its Johnson noise with a SQUID. A decoupling capacitor C_D is used to high pass filter the resistor noise, so the intrinsic noise of the SQUID can also be measured. The temperature of the thermal bath was calculated from the resistor noise with $I_b = 0 A$.

The results for a shunt resistor without cooling fins are shown on figure 3.16(a). The electron system temperature was calculated from average the of PSD noise above

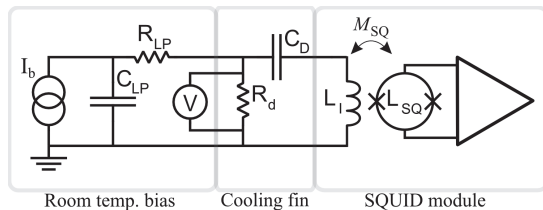


Figure 3.15: Scheme of the measurement setup. The shunt resistor R_d is biased by a current source I_b . The voltage drop across the resistor is measured by a room temperature voltmeter, connected in a four-terminal scheme. The temperature of the resistor is evaluated by measurement of its Johnson noise with a SQUID. A decoupling capacitor C_D is used to high pass filter the resistor noise, so the intrinsic noise of the SQUID can also be measured.

cutoff frequency of the decoupling capacitor C_D . For low power dissipation ($P \leq 1 \text{ nW}$) the fitted exponent value $p = 5.05$ is in a good agreement with reported results for thin PdAu resistors [58]. At a higher power however, the experimental data deviates from a theoretical curve with $p = 5$. At a middle temperature range the data can be refitted with $p = 5$ and the effective volume, which only includes the part of the resistor not covered by superconducting Nb pads. At even higher temperature ($> 1 \text{ K}$) the phonon system of the resistor can not be considered two dimensional, so higher dimensionality [59] and Kapitza resistance should be taken in to account [60].

The results of an identical experiment for a shunt resistor with cooling fins of tree different geometries are shown on figure 3.16(b). We can see that while the cooling fins help cooling the shunt resistors, at the power typically dissipated by the SQUID ($\approx 500 \text{ pW}$) the effect is negligible. From the theoretical and numerical studies presented in [55] one can conclude that the cooling fins are only effective at low temperature, low power conditions. At higher temperatures, limited by the SQUID dissipation, the cooling volume is restricted by the temperature dependent thermal relaxation length. In conclusion, in order to achieve the minimal working temperature one should maximize the volume of the dissipating part of the actual resistor. A possible solution is either bulk or implanted into silicon [61, 62] resistor. Another option is direct active cooling of the electron system. A recent work [63] has demonstrated a cooling power of $\approx 20 \text{ pW}$ per junction area of $0.3 \mu\text{m}^2$ at 1 K . A resulting cooling power density is $\sim 65 \text{ pW}/\mu\text{m}^2$, comparable with the power dissipated by the SQUID.

3.5.5 Transformer boxes noise

Before mounting the assembled transformer boxes on the MiniGRAIL setup we have measured the temperature dependence of the SQUID noise. The measurements were done in vacuum in liquid He cryostat. By pumping on the helium bath we have reached the minimum temperature of 1.6 K . The input terminals of the primary coil of the transformer were shorted by a superconducting wire. The noise curves of

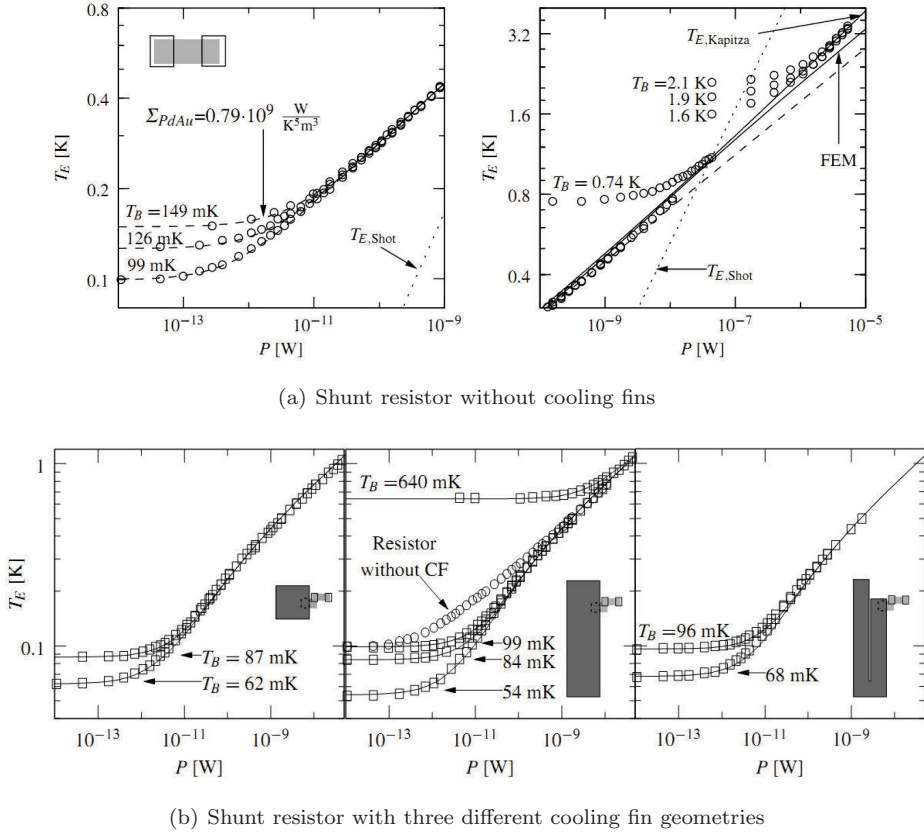


Figure 3.16: Temperature of the shunt resistor as a function of dissipated power [60].

two transformer boxes are shown on figure 3.17. Box#3 has a dual stage Quantum Design SQUID module, provided by the Auriga group, and Box#5 has a QD and flux transformer SQUID module made in Leiden. The noise curves of our other transformers were similar to Box#5.

3.5.6 Implementing a “cold” damping network

For a SQUID, strongly coupled to a high-Q resonator, the parasitic coupling from the SQUID to the input circuit can introduce a negative impedance which will overcome the dissipative terms of the input impedance and the resonator will be constantly pumped making the SQUID operation impossible. A special damping network can be implemented to stabilize the SQUID operation [64, 65]. Because the new MiniGRAIL SQUID electronics is fully differential, we modified the RC damping network that was

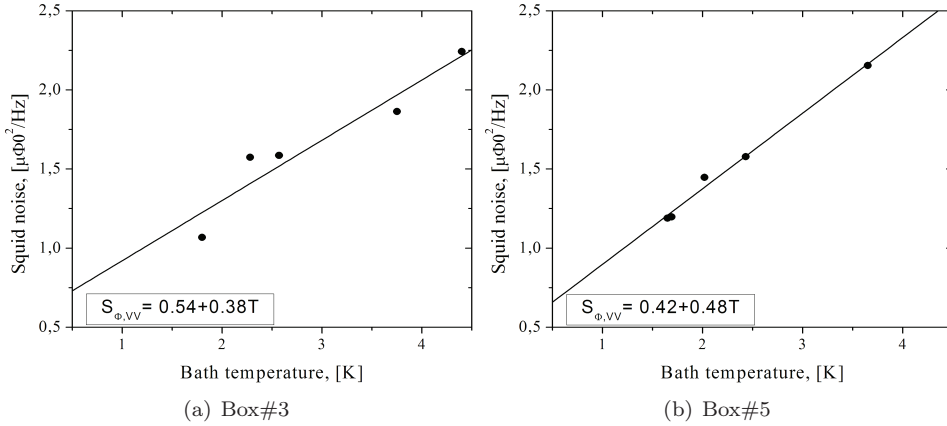


Figure 3.17: Flux noise of the two transformer boxes with shorted input. Box#3(a) has two Quantum Design DC SQUIDS and Box#5 has QD SQUID as a first stage and FT SQUID as an amplifier

used in the previous runs(see [25]).

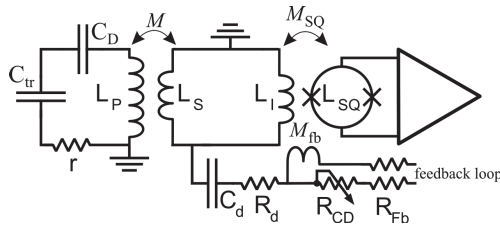


Figure 3.18: Schematics of a differential cold damping network.

The schematics of a modified damping network is shown on figure 3.18. $C_d = 10\text{ pF}$, $R_d = 0.35\text{ M}\Omega$. An extra resistor, R_{cd} creates an asymmetry in the Fb line, so that feedback coil is not at a zero potential anymore. So a small part of a Fb signal should leak to the ground through an RC line that introduces 90° phase shift in a signal. The cold damping network effect is equivalent to a series resistance r in the input circuit. We note that this additional resistance is the result of the feedback effect and therefore has no thermal noise associated with it. The effect of the cold damping network on the electrical mode Q factor and resonance frequency is given by [65]:

$$\Delta\left(\frac{1}{Q}\right) = \left(\frac{M}{L_t}\right)^2 \frac{L_i}{L_r} \frac{M_{SQ}}{M_{fb}} \frac{\omega_0 C_d}{1 + (\omega_0 R_d C_d)^2} R_{CD} \equiv \alpha R_{CD}$$

$$\Delta f_0 = \frac{f_0}{2} \left(\frac{M}{L_t}\right)^2 \frac{L_i}{L_r} \frac{M_{SQ}}{M_{fb}} \frac{(\omega_0 C_d)^2 R_d}{1 + (\omega_0 R_d C_d)^2} R_{CD} \equiv \beta R_{CD},$$
(3.3)

where $L_t = L_s + L_i$ is the total series inductance in the SQUID input circuit and $L_r = L_p - \frac{M^2}{L_t}$ is the reduced primary transformer inductance.

By changing the value of R_{cd} it is possible to reduce the quality factor of the electric mode to a reasonable value. The damping network was tested with the SQUID electronics during the short test cool-down of MiniGRAIL in 2008.

The change of the damping factor and the resonance frequency as a function of the value of the damping resistor, R_{cd} is shown on a figure 3.19

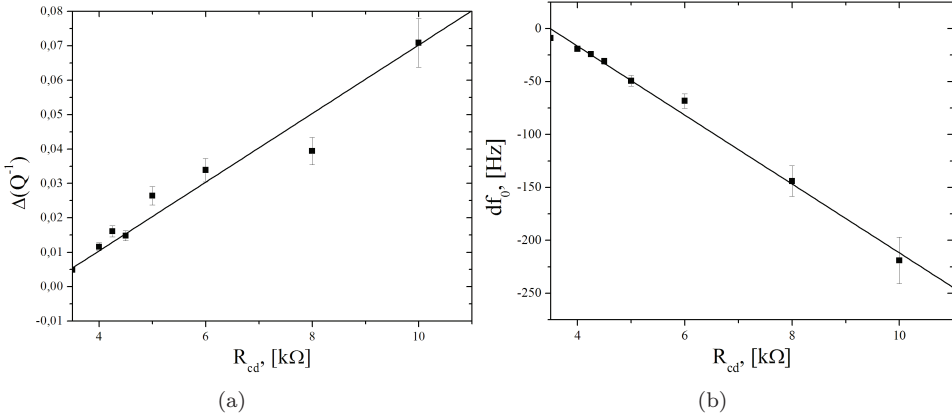


Figure 3.19: Effect of the cold damping on the electric mode quality factor (a) and resonance frequency (b)

3.6 Conclusions

In preparation to the big, 6 transducer run, we have tried to take into account and solve every problem we had during the previous cool-down:

- A multichannel acquisition system was developed and tested. It allows to store the acquired data together with the precise GPS timing information for later data analysis. An automatic SQUID reset electronics monitors the working point of the SQUID and resets the FLL integrator to relock the SQUID.

- Special effort was taken to improve the magnetic and RF shielding of the MiniGRAIL. This should improve the stability of the SQUID amplifiers.
- New transducers, with up to 5 times higher capacitance were developed. The new transducers can also be quickly disassembled and cleaned. This can be important, for operating 6 transducers simultaneously.
- Also new compact matching transformer boxes with the calibration coils were made.
- The DROSeS were replaced with custom design DC SQUIDs which were tested in dilution refrigerator. The measured noise was good enough to use them as the second stage amplifiers, or even as the first stage(Parallel washer design SQUID)